ADVANCED MATERIALS INTERFACES
Open Access
www.advmatinterfaces.de

Photodegradation and Thermal Effects in Violet Phosphorus

*Mahdi Ghafariasl, Sarabpreet Singh, Sampath Gamage, Timothy Prusnick, Michael Snure, and Yohannes Abate**

Violet phosphorus (VP) is garnering attention for its appealing physical properties and potential applications in optoelectronics. A comprehensive investigation of the photodegradation and thermal effects of exfoliated VP on SiO_2/Si substrates is presented. The degradation rate of VP is strongly influenced by the wavelength and exposure duration of light. Light illumination of VP above the bandgap leads to faster degradation, attributed to interactions with reactive oxygen species. Power-dependent photoluminescence (PL) measurements at low temperature (T = 4 K) show neutral exciton (X^0) and trion (T) intensities linearly increase with excitation power, while the energy difference between peak energies decreases. The T/X^0 spectral weight ratio increases from 0.28 at 300 K to 0.69 at 4 K, suggesting enhanced T formation due to reduced phonon scattering. Temperature-dependent Raman is used to investigate the phonon properties of VP. Tracking peak positions of 9 Raman modes with temperature, the linear first-order temperature coefficient is obtained and found to be linear for all modes. The results provide a deeper understanding of VP's degradation behavior and implications for optoelectronic applications.

1. Introduction

The ongoing evolution of the rich phase diagram of phosphorus allotropes, paired with the successful synthesis of these structures, has sparked increasing interest and opened avenues for diverse fundamental research and applications.[1–11] Among these is violet phosphorus (VP), a layered p-type semiconductor with a bandgap tunable in the range of 1.5 −2.5 eV.[5,12–14] Recently research has focused on various aspects of VP degradation under different environmental conditions.[9,15–19] Various factors including substrate hydrophobicity and surface roughness can influence VP's stability.[20] Although VP exhibits greater stability under ambient conditions compared to black phosphorus (BP),[21] like with BP, oxygen and water play a major role in the degradation of VP,[13] and needle-shaped VP has also been used as a catalyst.[22] Thermal degradation studies have also explored the evolution of Raman modes, some of which exhibit non-linear temperature dependence.[23]

In layered materials like transition metal dichalcogenides (TMDCs) such as MoS_2,[24–27] or other exfoliable materials like GaSe,[28] excitons dominate their optical properties at room temperature, which is a testament to their strong binding energy. Excitonic species have been observed in phosphorus allotropes like BP, with near-infrared emissions.[29,30] Conversely, VP emerges as an alternative with visible range photoluminescence (PL) emissions and higher thermal stability,[17,21] yet the investigation into its excitonic effects remains nascent.

In this work, we studied the photodegradation, thermal effects, and exciton emissions of exfoliated VP on SiO_2/Si substrates using atomic force microscopy (AFM), Raman, and PL spectroscopy across a range of temperatures and wavelengths. Our findings revealed that the degradation rate of VP is strongly influenced by wavelength and exposure duration of light. Above VP's bandgap light excitation was found to cause faster degradation due to interactions with reactive oxygen species (ROS). PL spectroscopy showed a gradual decline in the exciton population, suggesting reduced lifetime and alterations in the formation and stability of excitons, impacting VP's quantum efficiency. Power-dependent μ-PL measurements demonstrated intensity increases linearly for neutral excitons and trions, while the energy difference between their peak energies decreased with increasing power, indicative of changes in the exciton energy gap. Temperature-dependent PL revealed visible X^0 and T peaks, with a higher spectral weight of X^0 emission at elevated temperatures, implying reduced thermal stability of T emission in VP crystals. Temperature-dependent Raman spectroscopy was employed and peak positions of nine Raman modes were identified across varying temperatures up to

M. Ghafariasl, S. Singh, S. Gamage, Y. Abate
Department of Physics and Astronomy
University of Georgia
Athens, GA 30602, USA
E-mail: yohannes.abate@uga.edu
T. Prusnick
KBR
Beavercreek, OH 45433, USA
M. Snure
Air Force Research Laboratory
Sensors Directorate
Wright Patterson Air Force Base
Dayton, OH 45433, USA

The ORCID identification number(s) for the author(s) of this article can be found under https://doi.org/10.1002/admi.202300794

DOI: 10.1002/admi.202300794

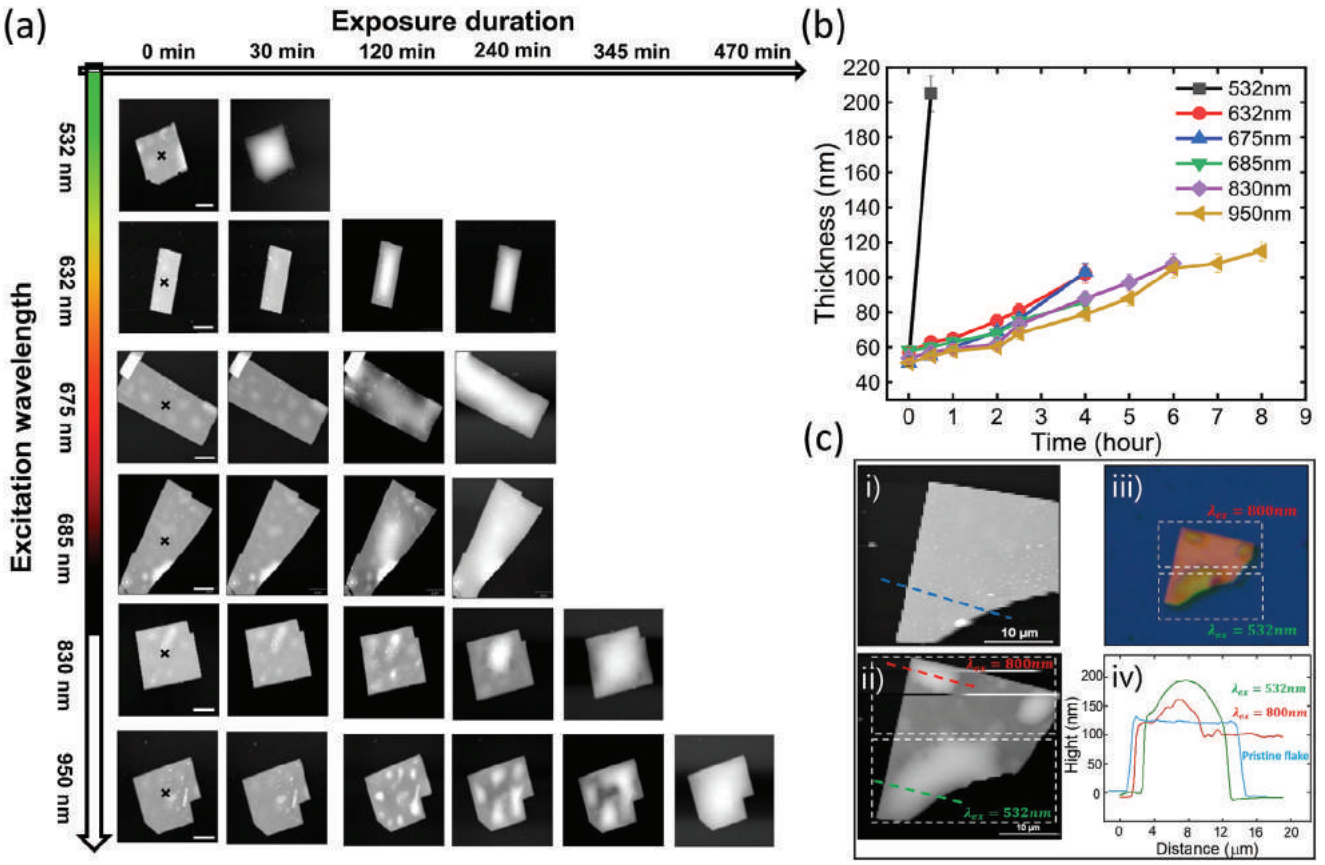

Figure 1. The effect of light wavelength and exposure time on VP degradation. a) AFM topography images of flakes as a function of time for different wavelengths. Degradation is manifested by the appearance and growth of bubble-like morphological features on the topography images. b) Topography height changes (thickness) measured at the center of flakes (marked by x on topography images) as a function of time for different laser wavelengths. c) Topography and optical images of a VP flake exposed to two different wavelengths. Topography of the pristine VP flake (i) and topography after exposure to 532 and 800 nm (ii). Optical image of the flake after exposing to two different lasers (iii), and line profiles of the different areas (iv).

675 K, leading to the determination of a linear first-order temperature coefficient consistent across all modes.

2. Results and Discussion

2.1. Excitation Laser Wavelength Dependent Photodegradation

We investigate the effect of laser wavelength on the degradation of VP flakes in the visible to NIR spectral range. To that end, we prepared six VP (HQ Graphene) flakes of similar thicknesses between 50 and 55 nm by exfoliation on SiO_2/Si substrates. Flakes were then exposed to lasers with different wavelengths followed by AFM topographic measurements overtime (**Figure 1a**). For all wavelengths used: 532, 632, 675, 685, 830, and 950 nm, the power and exposure time were kept similar. Laser exposure and AFM imaging of each flake was conducted in a dark room to rule out the influence of external light. As the VP surface degrades, bubble-like features form due to phosphorus oxide formation that eventually covers the entire flake. This results, as demonstrated in previous works, in a topographic height increase, which is a clear indication of degradation as shown in the AFM images in Figure 1a,b.[13,21,31–33] The flake exposed to 532 nm degrades the fastest, oxidizing after 30 min (thickness changes as large as a factor of≈ 4). Flakes exposed to 632, 675, and 685 nm all have much slower degradation rates (Figure 1a,b). The flake exposed to 830 nm remained partially intact after 6 h, while the flake subjected to 950 nm lasted for 8 h under similar conditions. We find that the longer laser wavelength (going from 532 to 950 nm), the slower the degradation rate (see also Figure S1, Supporting Information). To further compare the effect of laser wavelength on VP degradation rate, we exposed the same flake to two different laser excitation wavelengths, first with a 532 nm laser followed by an 800 nm laser. The topography of the flake before and after these two exposures is shown in Figure 1c. The top left section (i) of Figure 1c illustrates the topography of the pristine VP flake, while section (ii) showcases the topography of the flake after exposure to two wavelengths. Initially, we exposed the top side of the VP flake to 800 nm light for ≈2 h, after which we imaged the flake's topography. Subsequently, we exposed the bottom side of the same flake to 532 nm light for 30 min, followed by imaging the flake's topography. The optical image of the flake after exposure to these two distinct lights is presented in Figure 1c(iii). Figure 1c(iv) exhibits the line profiles from three different areas, which substantiate the effect of laser wavelength on degradation.

To further investigate the photodegradation of VP, we tracked the Raman intensity of 12, 45, 11, and 35 nm thick flakes

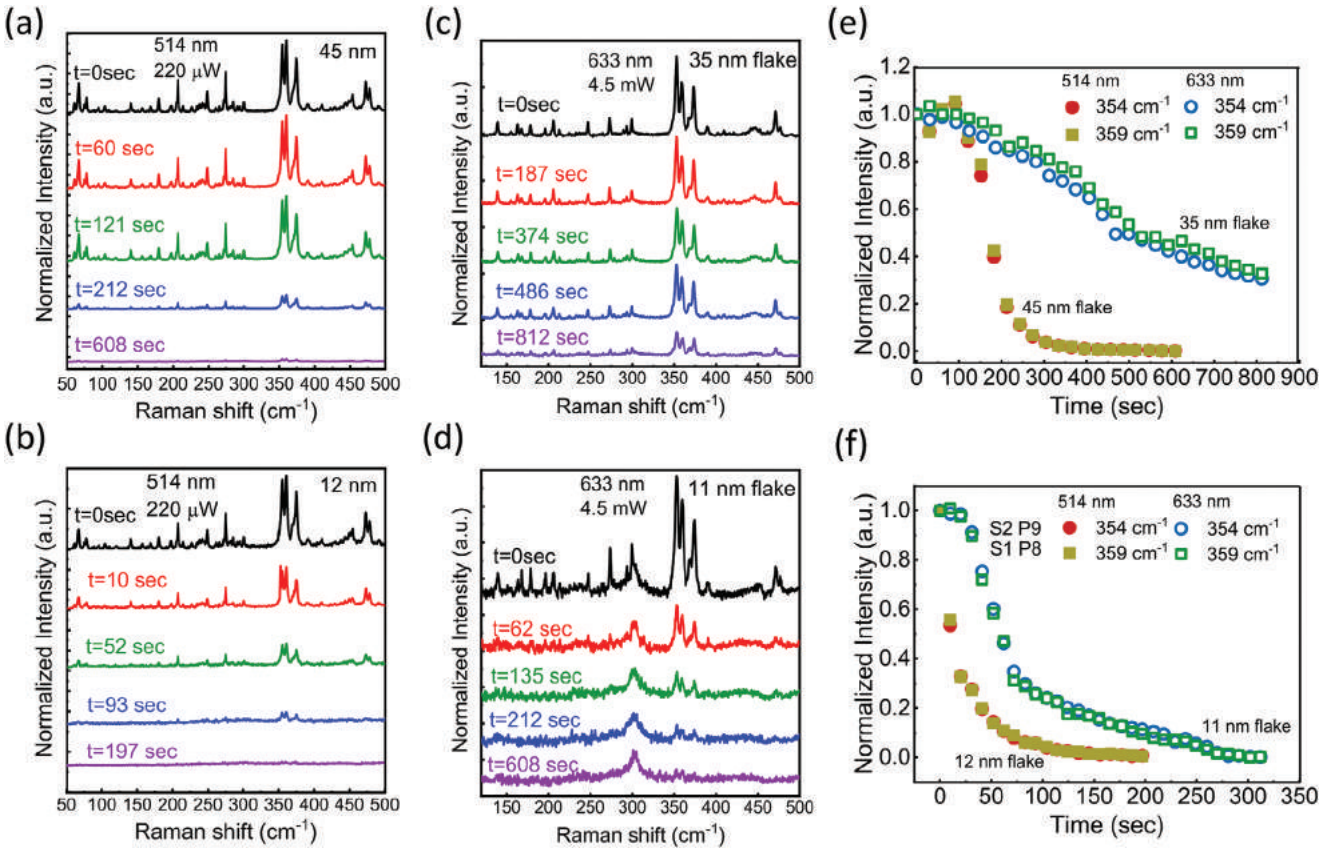

Figure 2. Laser accelerated degradation process. Raman spectra from a) 45 nm and b) 12 nm VP flakes on SiO_2/Si substrate exposed to 220 μW 514 nm laser and c) 35 nm and d) 11 nm VP flakes on SiO_2/Si substrate exposed to 4.5 mW 633 nm laser over time. Spectra was normalized by setting the Si peak to 1. Evolution of Raman intensity of the 354 and 395 cm^{-1} peaks over time under exposure to 514 or 633 nm lasers e) 45 and 35 nm and f) 12 and 11 nm flake. The intensity was normalized to t = 0 s. peak intensity.

exfoliated onto SiO_2/Si substrates under continuous exposure to either a 514 nm (power ≈220 μW) or 633 nm (power≈ 4.5 mW) laser, which are above and near the bandgap of VP. At the start of the experiment, all flakes showed the typical VP Raman spectra, which contain numerous modes ranging from 100 to 300 cm^{-1} and 350 to 500 cm^{-1} originating from VP's complex monoclinic crystal structure P2/n (13, C_{2h}(2/m)).[23] To compare all spectra, intensities were normalized by setting the Si substrate peak at ≈520 cm^{-1} to 1. **Figure** 2a–d shows the evolution of Raman spectra with time for the 45 and 12 nm thick flakes exposed to the 514 nm laser and 35 and 11 nm thick flakes exposed to the 633 nm laser. Figure 2e,f shows how the normalized intensity of the two most intense VP modes, 354 (S2 P9) and 359 (S1 P8) cm^{-1}, change with exposure to the 514 and 633 nm laser with time. Upon exposure to the 514 nm laser, the degradation process is quite rapid compared to the 633 nm consistent with the wavelength dependent photo-induced degradation observed using AFM. Under exposure to the 514 nm laser, the spectra of the 45 nm flake remain mostly unchanged for the first 90 s. Afterward, the intensity decreases rapidly until $t \approx 350$ s when it reaches ≈2% of the starting intensity. The intensity continues to decrease slowly becoming vanishingly low by 608 s. In the 12 nm flake, the intensity immediately decreases reaching <2% of the starting intensity in <114 s followed by a continuous slow decrease. As a comparison, the 11 and 35 nm flakes, which are exposed to the 633 nm laser at much higher power, show a significantly slower decrease in intensity. In the 11 nm thick film, it takes more than 280 s of exposure for the intensity to reduce to <2% of the initial, while the intensity of the 35 nm flake reduces to 30% after 800 s. As the flakes degrade no new Raman peaks appear and only VP-related peaks are observed with reducing intensity. The expected surface phosphorus oxide species (P_xO_y) that have previously been observed[21] are not known to be Raman active, thus we would not expect the emergence of new peaks similar to degradation studies on black phosphorus.[34]

Based on excitation wavelength dependence studies in Figures 1 and 2, we conclude that when VP is exposed to light with energy greater than its bandgap, excited electrons and holes can create reactive species such as free radicals,[35,36] which can oxidize VP enhancing its degradation. Ahmed et al.[32] have shown that UV light is predominantly responsible for the degradation of BP compared to longer excitation wavelengths. We find similar wavelength dependent degradation of VP suggesting ROS generation could play a role in VP degradation consistent with BP.[36] We note however, as reported before,[21] VP degrades slower than BP (see Figure S3, Supporting Information, for comparison under similar experimental conditions).

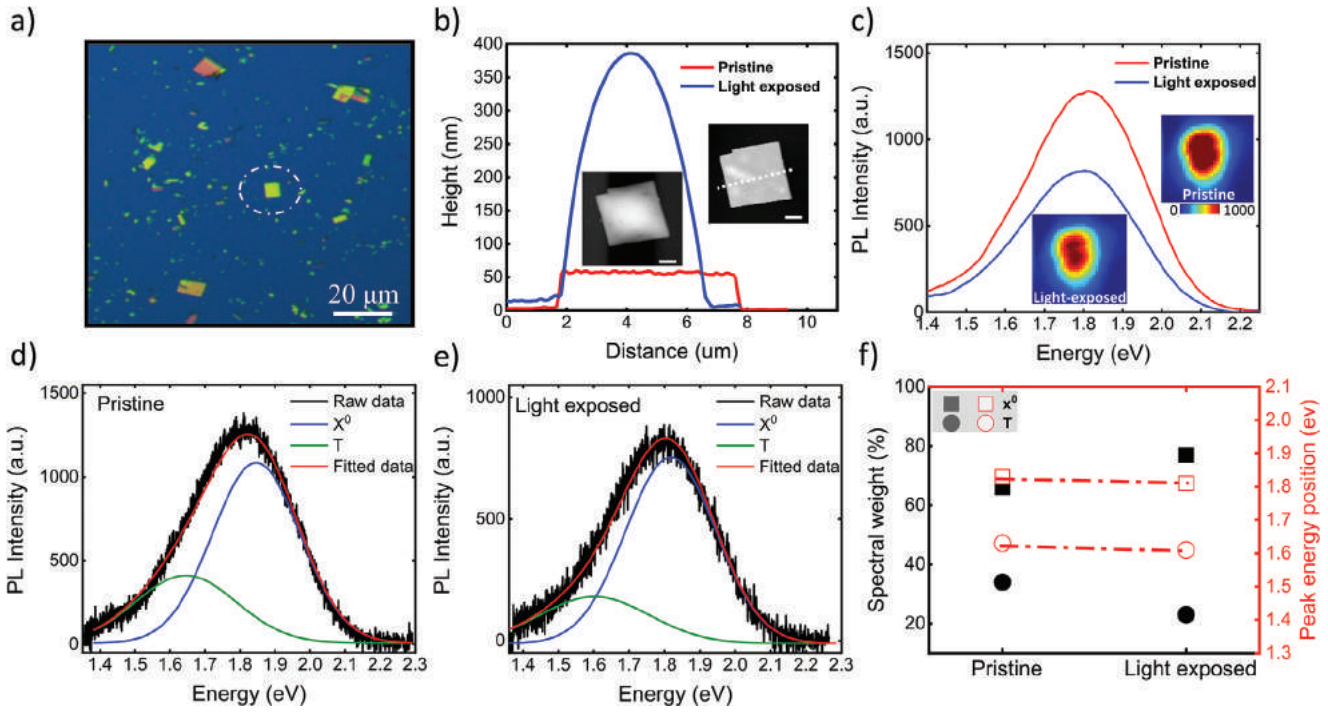

Figure 3. Topography and PL spectra of a VP flake overtime at room temperature. a) Optical image of the VP flakes on SiO_2 substrate. b) Topography and line-profile images of the pristine and light exposed flake. c) PL spectra of pristine and light exposed VP flake. The inset images show corresponding hyperspectral PL images for pristine and light exposed flake. d) Fitted data of PL spectra for pristine VP and e) light exposed VP. f) Peak weight (black) and peak energy position (red) of the X^0 (square) and T (circle) emissions as a function of the time for the pristine and light exposed VP flake. The wavelength of the excitation laser is 532 nm. Scale bars in b) denote 5 μm.

2.2. Excitons in VP

To understand the effect of degradation on light emission of VP, we performed PL spectroscopy as a function of excitation power and temperature over time. **Figure 3**b shows the topography change of a 60 nm exfoliated VP (indicated by a circle in the optical image in Figure 3a) on SiO_2/Si after exposure to a 532 nm laser of 0.3 mW for 30 min, the flake degrades substantially with a thickness increase to 385 nm. In Figure 3c, the PL spectra show that after light exposure, the intensity counts decrease compared to the pristine sample. Figure 3c insets show 2D spatial maps extracted from hyperspectral PL data cubes (Figure S2, Supporting Information). Although the hyperspectral map resolution is diffraction limited, it still reproduces the topographic shape revealing homogeneous intensity changes due to light exposure. To further analyze the excitonic species of VP, we fit PL spectra taken at the center of the flake using a dual-Gaussian function for the pristine and light-exposed flake shown in Figure 3d,e. For the pristine flake, the prominent peak (blue) at 1.82 eV is assigned as the neutral exciton (X^0) emission, while the left shoulder peak (green) at 1.63 eV is ascribed to the charged exciton or trion (T) emission.[17] After light exposure, the neutral exciton peak appears at 1.81 eV, and the T peak at 1.61 eV. Figure 3f (right panel), shows the peak energy position for both X^0 and T for the pristine VP flake and light exposed flake. The changes in peak position for both X^0 and T are negligible due to uncertainties in the spectral fitting. However, as the exposure time increases, the T emission gradually decreases compared to the initial state. Based on the fitted curve areas we calculated the peak weights[17,27] which are the ratio of the T ($\frac{T}{T+X^0}$) and the ratio of X^0 ($\frac{X^0}{T+X^0}$). The PL spectral weights of the X^0 and T emissions gradually change from X^0: 66%, T: 34% for the pristine sample to X^0: 77%, T: 23% for the degraded sample, Figure 3f (left panel), suggesting a gradual decline in T population.

Analysis of the full width at half maximum (FWHM) of the Gaussian fits to the PL peaks (Figure S4) shows the X° FWHM increases from 294 meV for pristine to 299 meV (light exposed), and the FWHM of T peak from 339 meV for pristine to 365 meV (light exposed). The large broadening in the FWHM of the T peak implies that the T is more susceptible to defects. Degradation lessens exciton lifetime through faster recombination and alters their formation and stability, impacting quantum efficiency.

2.3. Power Dependence of PL Spectra

The evolution of the PL spectra as a function of the excitation power gives information concerning the nature of the observed emissions. To that end, we have measured the power-dependent evolution of the PL spectra of a VP flake at $T = 4$ K using a 532 nm excitation with different laser powers, **Figure 4**. Dual-Gaussian was used to fit the integrated PL spectra and extract the spectral components of these two peaks, indicated by black dash lines in Figure 4a. The PL peak energy position of the X^0 and T emissions is found to be a function of the excitation laser power in Figure 4b. When the excitation power changes from 5 to 100 μW, the

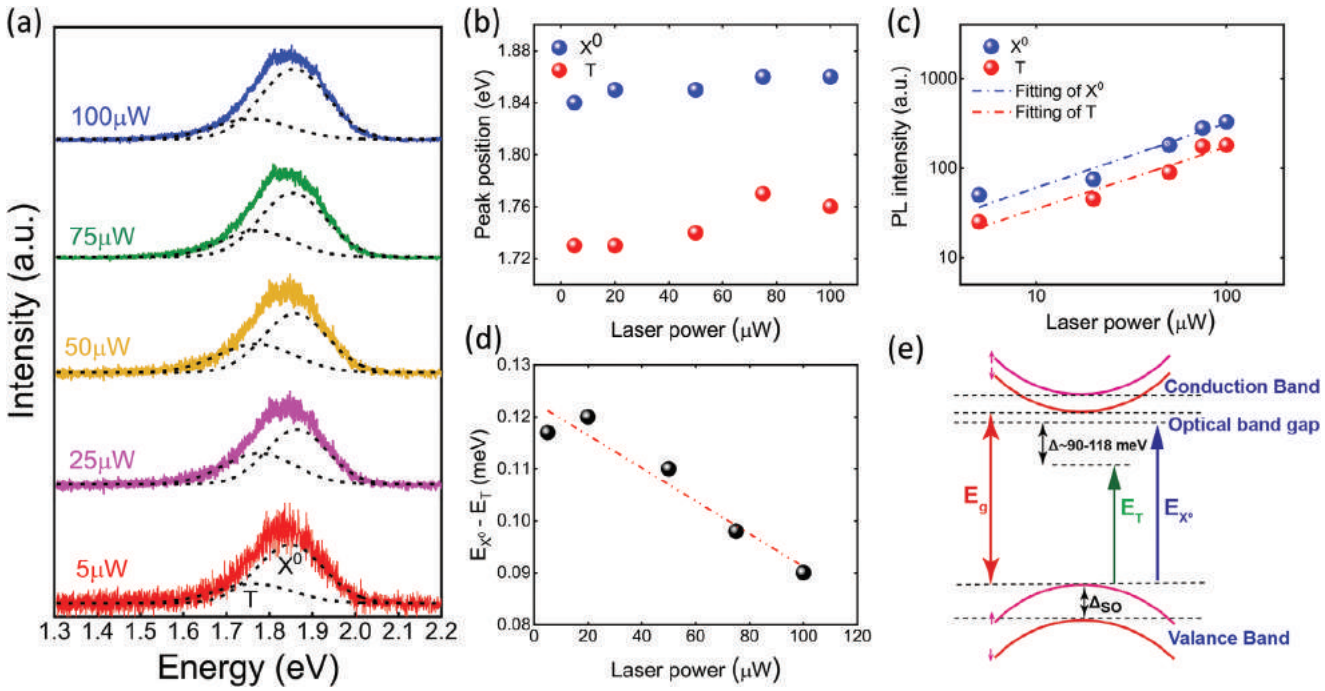

Figure 4. Laser power dependent X^0 and T emissions at low temperature ($T = 4$ K). a) PL spectra at different excitation laser powers. The black dashed lines are based on the dual-Gaussian fitting. b) Peak positions at different excitation laser powers. c) Integrated PL intensities for two peaks at different excitation laser powers, dashed lines show linear fits for two peaks. d) The difference in the PL peak energies of X^0 and T in (a), $E_{X^0} - E_T$ (symbols), as a function of excitation power. The red dashed line is a linear fit to the laser power dependence. e) Schematics of the energy diagram for X^0 and T of VP.

optical gap of the X^0 increases by ≈15 meV, and by ≈33 meV for the T. As the density of the photoexcited carriers increases with excitation power, the quasi-Fermi levels for electrons and holes shift respectively into the conduction and valence bands leading to a blue shift as reported for other 2D materials.[37–39] However, heating or strain-induced band variation could give rise to the reduced bandgap, exciton binding energy, and a redshift of the excitonic peaks.[40,41] Figure 4c shows the PL intensities at different powers for both X^0 and T peaks in VP. Based on the fitted data at different exciton powers, both intensities increase approximately linearly with the power, as demonstrated by the fits to the power law $I = P^k$, with $k = 0.88$ for neutral exciton and $k = 0.79$ for T peak. Figure 4d shows the difference in the PL peak energies of excitons ($E_X{}^0$) and trions (E_T), $E_X{}^0 - E_T$, as a function of laser excitation power. The linear fit to the laser power dependence (red dashed line) in Figure 4d shows PL intensities of the X^0 and T as a function of the laser power. Interestingly, the energy difference decreases from ≈118 to ≈90 meV as excitation power increases, which is due to changes in the exciton energy levels caused by photodegradation at higher powers.[30] However, it is been reported that the T peak saturates at high laser powers (≈2 mW).[17]

2.4. Temperature-Dependence of PL Spectra

Figure 5a depicts the evolution of temperature-dependent PL spectra of VP flake thickness 60 nm when excited by a 532 nm laser. At a temperature of 304 K, visible X^0 and T peak components can be seen, with a greater spectral weight of X^0 emission, indicating reduced thermal stability of T, similar effects have also been seen in BP and MoS_2.[42,43] Both the X^0 and T emissions increase as the temperature is decreased to 4 K, which is attributed to less phonon scattering.[44] The peak position energies of X^0 and T obtained by dual Gaussian fitting are shown in Figure 5b. With increasing temperature, optical transition energies (peak positions) show a red shift as expected from the temperature dependence of the bandgap. To fit the experimental peak positions of X^0 and T at different temperatures, we applied the O'Donnell equation, which predicts the temperature-dependent bandgap of semiconductors based on electron–phonon interaction.[45,46]

$$E_g(T) = E_g(0) - S\langle\hbar\omega\rangle\left[\coth\left(\frac{\langle\hbar\omega\rangle}{2kT}\right) - 1\right] \quad (1)$$

where $E_g(0)$ is the ground-state transition energy at 0 K, S is a dimensionless coupling constant and $\langle\hbar\omega\rangle$ is an average phonon's energy. According to the fitting lines, the $E_g(0)$ for X^0 and T emission energies are 1.86 and 1.75 eV at 4 K, respectively. The trion dissociation energy $\langle\Delta\hbar\omega\rangle$ that represents the energy difference between the X^0 and T peaks in the PL spectrum, is determined to be 110 meV at 4 K. The dissociation energy steadily increases to 260 meV at 304 K as the temperature rises consistent with previous reports.[17]

As the temperature is reduced (300 to 4 K) the ratio of the spectral weight of the T to X^0 (T/X^0) changes from 0.28 at 300 K to 0.69 (Figure 5c). The significant increase in the T spectral weight at low temperatures implies the formation of more T, which might be associated with the weakening of phonon scattering. The maximum spectral weight of the T/X^0 ratio at 4 K measured for two

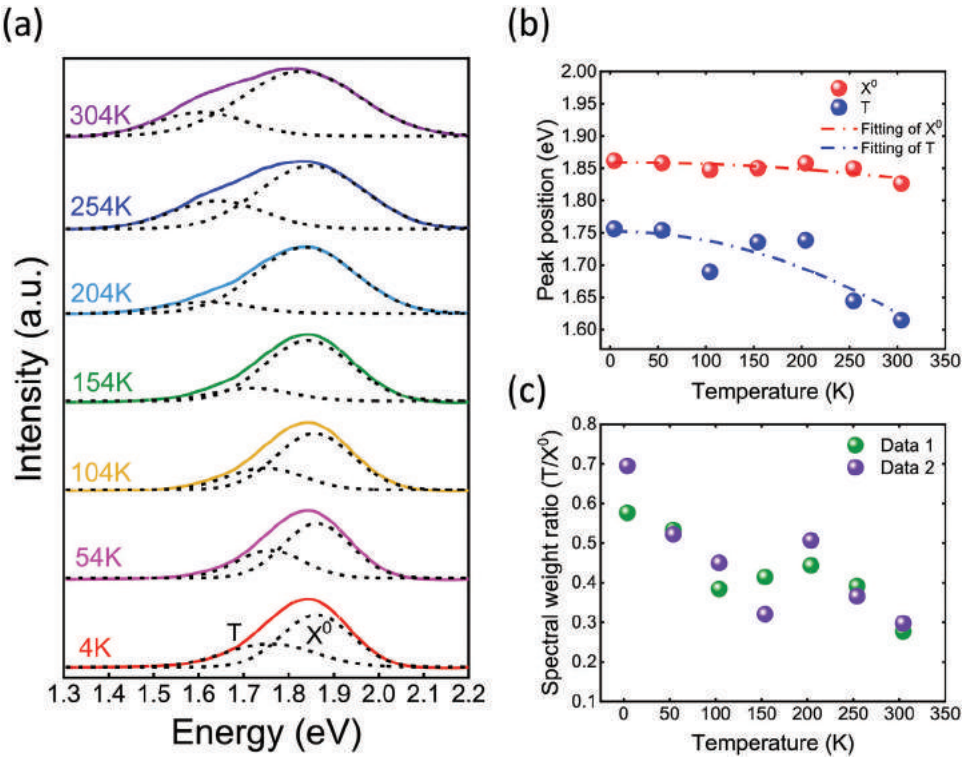

Figure 5. a) Temperature-dependent evolution of VP PL spectra by representative deconvolution of the X^0 and T (black dash lines are fitting curves) emission components. b) peak position of X^0 and T at different temperatures. The dash lines are fitted data. c) Spectral weight ratio as a function of temperature.

different flakes was 0.69 and 0.59 comparable to other works.[17] Similar effects has been observed in other 2D materials (few layered MoS_2), where T emission was found to be more prominent compared to the X^0 emission.[26] The T peak is more sensitive to temperature changes than the exciton PL band that can likely be ascribed to the enhanced non-radiative recombination channels, which are more active due to the increased electron–phonon interactions at higher temperatures. This sensitivity is primarily due to their relatively lower binding energy compared to X^0, making T emissions more susceptible to thermal effects. The interaction with phonons becomes more significant at higher temperatures, leading to increased scattering and dissociation of T in VP. Investigation of the temperature dependence of the X^0 and T FWHM (Figure S7, Supporting Information) exhibits a large increase indicating a substantial broadening with rising temperature as observed in other 2D materials.[27,28,44,47,48]

Finally, we investigate the temperature-dependent phonon properties of VP using temperature-dependent Raman from 173 to 673 K under an inert N_2 environment. Two VP flakes exfoliated on SiO_2/Si with thicknesses of 23 and 53 nm were characterized. **Figure** 6a shows the evolution of the Raman spectra with temperature increasing from 173 to 673 K and back down to 303 K on the 23 nm thick flake. As the temperature increased a clear broadening and red shifting of peaks was observed with many of the peaks merging. At 673 K, a new broad peak between 300 and 350 cm^{-1} begins to emerge, which becomes quite pronounced upon cooling back to 303 K. Not all peaks in the original spectra can be observed on cooling and the intensity of the observable peaks is much lower indicating degradation of the sample. Most striking is the emergence of two new broad peaks at ≈210 and 330 cm^{-1}. At this point, the origin of these peaks remains unknown and cannot be assigned to any of the known phosphorus allotropes or phosphorus species.[49]

The temperature-dependent shift for nine VP peaks from the 23 and 53 nm thick flakes are plotted in Figure 6b. All modes were found to have a linear temperature dependence and were fit to $\omega(T) = \omega(0) + \chi T$, which describes the first-order temperature coefficient χ. The peak position versus temperature for both flakes is consistent across the measured temperature range with χ ranging from 0.0083 to 0.0277 cm^{-1} deg^{-1}. These χ values are consistent with those reported by L. Zhang et al.[23] except for the T_g and P tube modes, which L. Zhang et al. found to have a nonlinear temperature dependence. However, we found the T_g and P_{tub} modes merged above 473 K making it challenging to accurately determine peak position. Upon cooling back to 303 K the peak positions were found to be only slightly lower than when measured during.

3. Conclusion

We report on a thorough investigation of the photo- and thermal-degradation of VP. Using a combination of AFM and Raman, we reveal VP degradation is accelerated by exposure to light with a rate strongly dependent on wavelength and exposure time. Flakes of similar thickness exposed to above VP's bandgap (>532 nm) degraded the fastest, while flakes exposed to sub-bandgap light

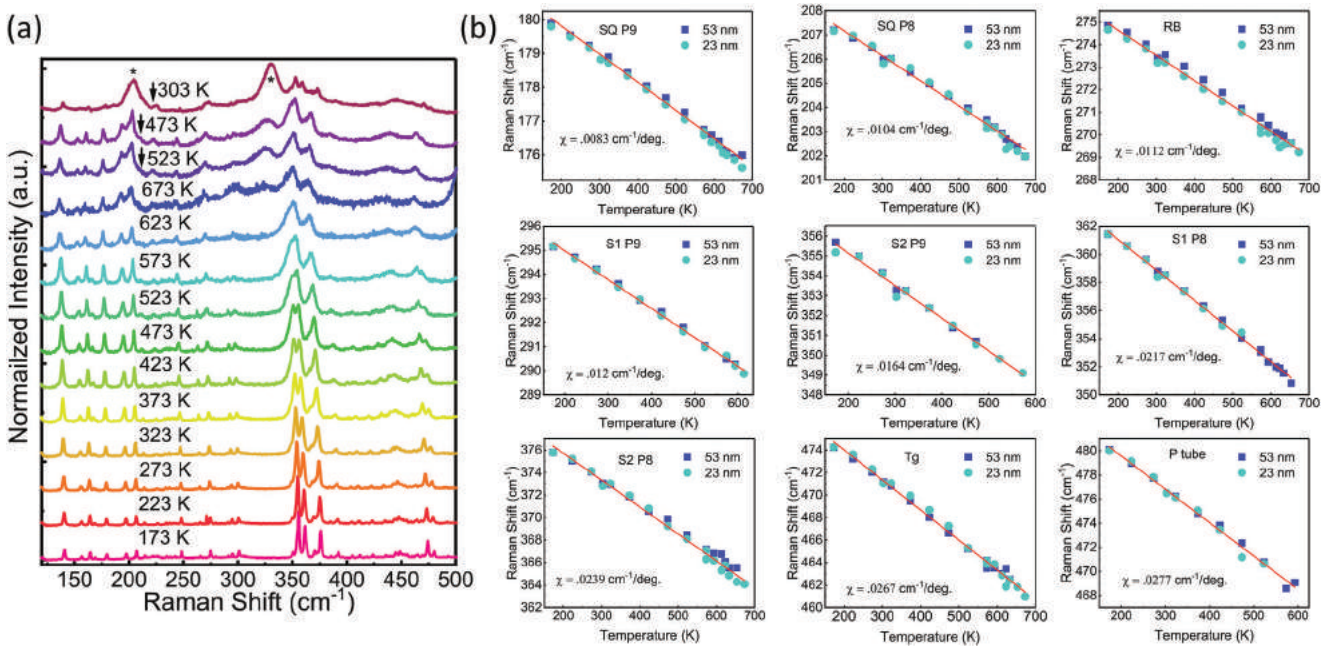

Figure 6. a) Normalized Raman spectra of violet phosphorus single crystals in a temperature range of 173–673 K. b) The temperature-dependent shift for nine VP peaks from the 23 and 53 nm thick flakes are plotted with the corresponding fitting lines.

degraded much slower. This photo-accelerated degradation is attributed to interactions with ROS. PL spectroscopy was performed as a function of time, power, and temperature to understand the effect of degradation on exciton emissions. Degradation can shorten the lifetime of excitons impacting exciton formation and stability. The T/X^0 spectral weight ratio increased at low temperatures, indicating enhanced T formation due to weakened phonon scattering. Temperature-dependent Raman was used to investigate the phonon properties of VP. VP flakes were shown to have a linear first-order temperature coefficient and survive up to 675 K with some irreversible degradation. Our findings elucidate the primary factors causing VP degradation, offering insights that will support the development of durable, long-lasting optoelectronic devices leveraging VP's unique properties.

4. Experimental Section

Sample Preparation: Violet phosphorus flakes were mechanically exfoliated from bulk samples obtained from HQ Graphene, which were produced by Chemical Vapor Transport (CVT). Flakes were exfoliated using adhesive tape and then quickly transferred onto SiO_2 substrates for characterization. The exfoliation was performed in the air and kept in a dark room.

Raman Measurements: Raman spectra were collected using Renishaw Inviva system 20 μm slits and 3000 line mm^{-1} grating. For temperature dependent measurements a Linkam environmental stage was used to control temperature under an N_2 environment and a 220 μW 633 nm excitation source was used. Samples were cooled to 173 K under flowing N_2, heated to 673 K, and cooled back to 303 K taking measurements both during heating and cooling. Measurements between 173 and 573 K were taken at 50° increments and 20° increments from 573 to 673 K. Before each measurement the temperature was stabilized for 10 min. For photodegradation measurements VP flakes were continuously exposed to either a 514 nm (power ≈220 μW) or 633 nm (power ≈4.5 mW) laser under an ambient atmosphere and Raman data were collected periodically.

Photoluminescence (PL) Measurements: Low-temperature PL spectra were measured using a confocal laser scanning microscope system equipped with a vibration-free closed-cycle cryostat (Attodry 800, Attocube). CW laser as an excitation source was focused into a small spot with a diameter of ≈2–3 μm on the sample through a 100× objective lens (APO/VIS, N.A. = 0.82; Attocube) inside the vacuum chamber. PL spectra were then collected through the same lens as the excitation beam and filtered using a long-pass filter before entering a spectrometer (Andor), which consists of a monochromator and a thermoelectrically cooled CCD camera. Topography and PL measurements at room temperature were acquired using a commercial AFM system (Attocube Co.). VP flakes were exposed to discrete wavelengths (532, 633, 565, 675, 685, 830, and 950 nm) from a commercial Matisse tunable laser pumped by a 532 nm CW laser (Spectra-Physics.Co.). Measurements were performed in a dark room to minimize the external light exposure.

Supporting Information

Supporting Information is available from the Wiley Online Library or from the author.

Acknowledgements

M.G., S.S., and Y.A. acknowledged support by the Air Force Office of Scientific Research (AFOSR) grant numbers FA9550-19-0252 and FA9550-23-1-0375. Partial support for S.G. came from the National Science Foundation (NSF) Grant No. 2152159 (NRT-QuaNTRASE). M.S. and T.P. acknowledged funding from the Air Force Office of Scientific Research (AFOSR) under award numbers FA9550-19RYCOR050 and FA9550-24RYCOR011.

Conflict of Interest

The authors declare no conflict of interest.

Data Availability Statement

The data that support the findings of this study are available on request from the corresponding author. The data are not publicly available due to privacy or ethical restrictions.

Keywords

layered structures, photodegradation, photoluminescence, Raman spectroscopy, violet phosphorus

Received: September 21, 2023
Revised: December 15, 2023
Published online:

[1] A. Pfitzner, *Angew. Chem., Int. Ed.* **2006**, *45*, 699.
[2] H. Huang, L. Zhang, B. Xiao, Y. Cheng, J. Zhang, *Appl. Phys. Lett.* **2019**, *115*, 163101.
[3] T. Nilges, P. Schmidt, R. Weihrich, in *Encyclopedia of Inorganic and Bioinorganic Chemistry* (Ed: R. A. Scott), Wiley, Hoboken, NJ **2011**, 1.
[4] Z. Zhu, D. Tománek, *Phys. Rev. Lett.* **2014**, *112*, 176802.
[5] L. Zhang, M. Gu, L. Li, X. Zhao, C. Fu, T. Liu, X. Xu, Y. Cheng, J. Zhang, *Chem. Mater.* **2020**, *32*, 7363.
[6] M. Ruck, D. Hoppe, B. Wahl, P. Simon, Y. Wang, G. Seifert, *Angew. Chem., Int. Ed.* **2005**, *44*, 7616.
[7] L. Li, Y. Yu, G. J. Ye, Q. Ge, X. Ou, H. Wu, D. Feng, X. H. Chen, Y. Zhang, *Nat. Nanotechnol.* **2014**, *9*, 372.
[8] N. Eckstein, A. Hohmann, R. Weihrich, T. Nilges, P. Schmidt, *Z. Anorg. Allgem. Chem.* **2013**, *639*, 2741.
[9] L. Zhang, H. Huang, B. Zhang, M. Gu, D. Zhao, X. Zhao, L. Li, J. Zhou, K. Wu, Y. Cheng, J. Zhang, *Angew. Chem. Int. Ed.* **2020**, *59*, 1074.
[10] Q. Liu, X. Zhang, J. Wang, Y. Zhang, S. Bian, Z. Cheng, N. Kang, H. Huang, S. Gu, Y. Wang, D. Liu, P. K. Chu, X.-F. Yu, *Angew. Chem.* **2020**, *132*, 14489.
[11] J. Guan, Z. Zhu, D. Tománek, *Phys. Rev. Lett.* **2014**, *113*, 226801.
[12] R. Zhao, S. Liu, X. Zhao, M. Gu, Y. Zhang, M. Jin, Y. Wang, Y. Cheng, J. Zhang, *J. Mater. Chem. A* **2022**, *10*, 245.
[13] J. Xue, S. Wang, J. Zhou, Q. Li, Z. Zhou, Q. Hui, Y. Hu, Z. Zhou, Z. Feng, Q. Yan, Y. Yu, Y. Weng, R. Tang, X. Su, Y. Xin, F. Zheng, S. Ju, L. You, L. Fang, *Appl. Phys. Lett.* **2023**, 122.
[14] F. Baumer, Y. Ma, C. Shen, A. Zhang, L. Chen, Y. Liu, D. Pfister, T. Nilges, C. Zhou, *ACS Nano* **2017**, *11*, 4105.
[15] S. Lin, W. K. Lai, Y. Li, W. Lu, G. Bai, S. P. Lau, *SmartMat* **2021**, *2*, 226.
[16] X. Liu, S. Wang, Z. Di, H. Wu, C. Liu, P. Zhou, *Adv. Sci.* **2023**, *10*, 2301851.
[17] Y. Li, S. Cai, W. K. Lai, C. Wang, L. Rogée, L. Zhuang, L. Zhai, S. Lin, M. Li, S. P. Lau, *Adv. Opt. Mater.* **2022**, *10*, 2101538.
[18] A. G. Ricciardulli, Y. Wang, S. Yang, P. Samorì, *J. Am. Chem. Soc.* **2022**, *144*, 3660.
[19] L. Jin, R. Guo, T. Han, R. Wang, Y. Zhang, *Adv. Funct. Mater.* **2023**, 33.
[20] S. Singh, M. Ghafariasl, H.-Y. Ko, S. Gamage, R. A. Distasio Jr, M. Snure, Y. Abate, *arXiv* **2023**, arXiv230617681.
[21] A. Fali, M. Snure, Y. Abate, *Appl. Phys. Lett.* **2021**, 118.
[22] M. Jin, Y. Wang, M. Gu, X. Zhao, R. Zhao, Y. Zhang, Y. Cheng, J. Zhang, *Nano Res.* **2022**, *16*, 3320.
[23] L. Zhang, H. Huang, Z. Lv, L. Li, M. Gu, X. Zhao, B. Zhang, Y. Cheng, J. Zhang, *ACS Appl. Electron. Mater.* **2021**, *3*, 1043.
[24] M. Tebyetekerwa, J. Zhang, Z. Xu, T. N. Truong, Z. Yin, Y. Lu, S. Ramakrishna, D. Macdonald, H. T. Nguyen, *ACS Nano* **2020**, *14*, 14579.
[25] A. Splendiani, L. Sun, Y. Zhang, T. Li, J. Kim, C.-Y. Chim, G. Galli, F. Wang, *Nano Lett.* **2010**, *10*, 1271.
[26] S. Golovynskyi, I. Irfan, M. Bosi, L. Seravalli, O. I. Datsenko, I. Golovynska, B. Li, D. Lin, J. Qu, *Appl. Surf. Sci.* **2020**, 515.
[27] S. Golovynskyi, O. I. Datsenko, D. Dong, Y. Lin, I. Irfan, B. Li, D. Lin, J. Qu, *J. Phys. Chem. C* **2021**, *125*, 17806.
[28] M. Usman, S. Golovynskyi, D. Dong, Y. Lin, Z. Yue, M. Imran, B. Li, H. Wu, L. Wang, *J. Phys. Chem. C* **2022**, *126*, 10459.
[29] Z. Lin, Z. Tian, W. Cen, Q. Zeng, *Phys. B* **2023**, 657.
[30] A. Surrente, A. A. Mitioglu, K. Galkowski, W. Tabis, D. K. Maude, P. Plochocka, *Phys. Rev.* **2016** 93.
[31] S. Gamage, Z. Li, V. S. Yakovlev, C. Lewis, H. Wang, S. B. Cronin, Y. Abate, *Adv. Mater. Interfaces* **2016**, *3*, 1600121.
[32] T. Ahmed, S. Balendhran, M. N. Karim, E. L. H. Mayes, M. R. Field, R. Ramanathan, M. Singh, V. Bansal, S. Sriram, M. Bhaskaran, S. Walia, *npj 2D Mater. Appl.* **2017**, *1*, 18.
[33] Y. Abate, S. Gamage, Z. Li, V. Babicheva, M. H. Javani, H. Wang, S. B. Cronin, M. I. Stockman, *Light. Sci. Appl.* **2016**, *5*, e16162.
[34] F. Alsaffar, S. Alodan, A. Alrasheed, A. Alhussain, N. Alrubaiq, A. Abbas, M. R. Amer, *Sci. Rep.* **2017**, *7*, 44540.
[35] M. Li, C. Mao, L. Ling, *Environ. Sci. Technol.* **2022**, *56*, 361.
[36] Q. Zhou, Q. Chen, Y. Tong, J. Wang, *Angew. Chem. Int. Ed.* **2016**, *55*, 11437.
[37] K. F. Mak, K. He, C. Lee, G. H. Lee, J. Hone, T. F. Heinz, J. Shan, *Nat. Mater.* **2013**, *12*, 207.
[38] M. Ghafariasl, T. Zhang, Z. D. Ward, D. Zhou, D. Sanchez, V. Swaminathan, H. Terrones, M. Terrones, Y. Abate, *arXiv* **2023**, arXiv:230814990.
[39] A. Chernikov, C. Ruppert, H. M. Hill, A. F. Rigosi, T. F. Heinz, *Nat. Photonics* **2015**, *9*, 466.
[40] N. Peimyoo, J. Shang, W. Yang, Y. Wang, C. Cong, T. Yu, *Nano Res.* **2014**, *8*, 1210.
[41] A. Steinhoff, M. Rösner, F. Jahnke, T. O. Wehling, C. Gies, *Nano Lett.* **2014**, *14*, 3743.
[42] G. Zhang, A. Chaves, S. Huang, F. Wang, Q. Xing, T. Low, H. Yan, *Sci. Adv.* **2018**, *4*, eaap9977.
[43] M. Florian, M. Hartmann, A. Steinhoff, J. Klein, A. W. Holleitner, J. J. Finley, T. O. Wehling, M. Kaniber, C. Gies, *Nano Lett.* **2018**, *18*, 2725.
[44] S. Sharma, S. Bhagat, J. Singh, M. Ahmad, S. Sharma, *J. Mater. Sci.: Mater. Electron.* **2018**, *29*, 20064.
[45] Y. P. Varshni, *Physica* **1967**, *34*, 149.
[46] A. A. Mitioglu, P. Plochocka, J. N. Jadczak, W. Escoffier, G. L. J. A. Rikken, L. Kulyuk, D. K. Maude, *Phys. Rev. B* **2013**, 88.
[47] J. W. Christopher, B. B. Goldberg, A. K. Swan, *Sci. Rep.* **2017**, *7*, 14062.
[48] J. Pei, J. Yang, R. Xu, Y.-H. Zeng, Y. W. Myint, S. Zhang, J.-C. Zheng, Q. Qin, X. Wang, W. Jiang, Y. Lu, *Small* **2015**, *11*, 6384.
[49] G. Abellán, S. Wild, V. Lloret, N. Scheuschner, R. Gillen, U. Mundloch, J. Maultzsch, M. Varela, F. Hauke, A. Hirsch, *J. Am. Chem. Soc.* **2017**, *139*, 10432.